Supplemental Data

The Processivity of Kinesin-2 Suggests Diminished Front-Head Gating

Gayatri Muthukrishnan, Yangrong Zhang, Shankar Shastry, William O. Hancock

Current Biology (2009)

Summary of Run Length and Velocity Data

Table S1 presents a summary of all of the run length and processivity data from bead assays at 1 mM ATP . The number of steps per run was calculated by dividing the run lengths by 8 nm, and the probability of motor unbinding per step was calculated as the inverse of the mean run length.

Table 1: Motor Run Lengths and Velocities at 1 mM ATP from Bead Assay

	KHC	KIF3A/B	KIF3A/A	KIF3B/B	KHC_{+DAL}
Run Length (nm) (mean ± SE, N)	1747 ± 199 (57)	449 ± 30 (88)	410 ± 35 (85)	704 ± 81 (83)	355 ± 14 (136)
Velocity (nm/s) (mean ± SD, N)	703 ± 136 (58)	436 ± 129 (90)	455 ± 115 (101)	458 ± 106 (102)	552 ± 103 (97)
Number of steps	218 ± 25	56 ± 4	51 ± 4	88 ± 10	44 ± 2
p_{unbind}	0.005	0.018	0.020	0.011	0.023

Repairing KIF3 plasmid sequences

In the course of these experiments, mutations were discovered in the KIF3 plasmids used previously [1]. These mutations were introduced during the construction of the plasmids. There were three mutations in the KIF3A head domain (Gly_{121} to Glu_{121}, Ala_{210} to Val_{210} and Pro_{296} to Ser_{296}) and one in the coiled-coil (Lys_{404} to Arg_{404}). KIF3B had one mutation in the head (Ala_{34} to Val_{34}) and the other in the coiled-coil (Ala_{465} to Val_{465}). The sequences were corrected using QuikChange® Multi Site-Directed Mutagenesis (Stratagene, Inc.) and all plasmids were sequenced to confirm repairs. When these sequence corrected motors were examined in microtubule gliding assays, the velocity differences seen previously were abolished [1].

Details of Bead Assays

560 nm diameter, carboxylated polystyrene beads (146 pM) (Bangs Laboratories, Inc.) were passivated with 4 mg mL^{-1} casein in BRB80 (80 mM PIPES, 1 mM $MgCl_2$, 1 mM EGTA, pH 6.8) and sonicated for 1 hr to prevent aggregation. Subsequently, motors were incubated with 14.6 pM casein-coated beads at 4°C for 30 min. Motor concentrations were determined by scanning Coomassie stained SDS-PAGE gels using a GelDoc system and comparing to a BSA control protein. Bovine brain tubulin was purified, rhodamine-labeled and polymerized following established techniques [2, 3]. Flow cells were constructed from microscope slides (Fisher Finest), clean glass coverslips (Corning), and two-sided tape. Microtubules were flowed in and allowed to bind to the glass coverslip, the surface was blocked with 2 mg mL^{-1} BSA, and, motor-functionalized beads diluted ten-fold in motility solution (10 μM paclitaxel, 0.2 mg mL^{-1} casein, 1 mM MgATP, 20 mM glucose, 0.02 mg mL^{-1} glucose oxidase, 0.008 mg mL^{-1} catalase, 0.5% β-mercaptoethanol in BRB80) were introduced. Beads and microtubules were observed simultaneously with DIC and epifluorescence on a Nikon TE2000 inverted microscope

(100X, 1.3 NA objective) with a Photometrics Cascade 512B CCD camera (Roper Scientific). Images and movies were recorded using Meta-Vue (Universal Imaging).

To facilitate motor-microtubule interactions, an optical trap was built to grab beads and bring them in contact with microtubules. The trap system consists of a 1064 nm Nd-YAG 10W laser (Spectra-Physics) operated at 2 W output power, a 10x beam expander, and a half-wave plate and beam-splitter for power attenuation. The laser enters the rear of the Nikon TE2000 microscope, passes through the epifluorescence pathway and fills the back aperture of the 100x 1.3 NA objective. A back focal plane interferometry detection system was constructed to calibrate the trap stiffness. The stiffness was set between 0.002 and 0.008 pN nm^{-1} (over a linear range of approximately 130 nm) for all experiments. The load conditions at this stiffness are negligible considering the 6 pN stall force of Kinesin-1 [4].

To confirm that bead movements resulted from single motors, beads were trapped in solution and placed on microtubules for 30 s. The fraction of beads that moved was plotted against motor-to-bead ratio, and was fit to the Poisson probability of a bead having one or more motors, i.e., $P(n \geq 1) = 1 - P(0) = 1 - \exp(-x/k)$, where x is the number of motors per bead and k is a functional parameter that relates the number of total motors/bead to the number of functional motors/bead [4, 5]. Data for KHC and KIF3A/B are shown in Figure S1 For all subsequent experiments, motor concentrations were chosen such that ≤ 20% beads moved, ensuring single motor interactions. These working motor concentrations (incubated with 14.6 pN beads) were 34 pM (KHC), 22 pM (KIF3A/B), 25 pM (KIF3A/A), and 22 pM (KIF3B/B).

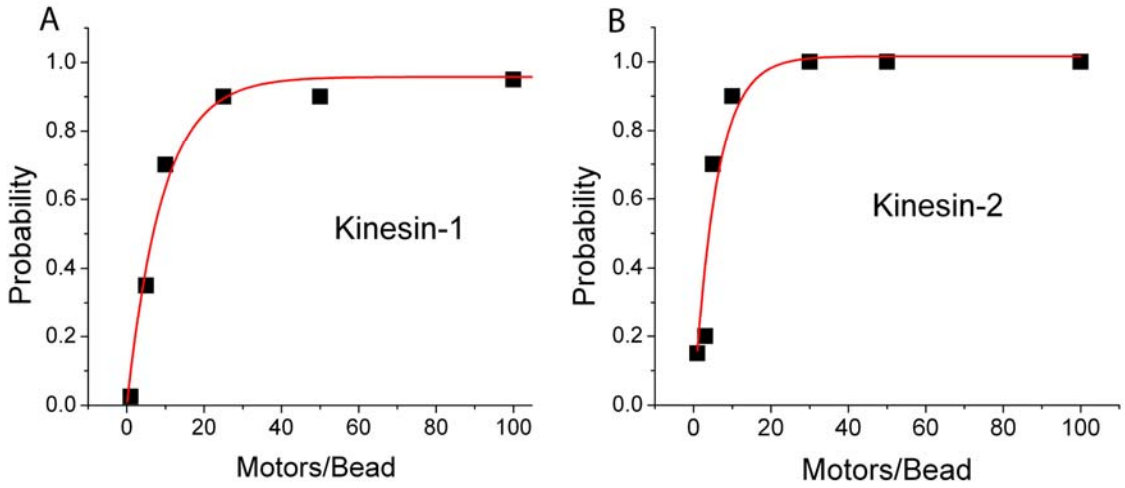

Figure S1: Dilution profiles of A) Kinesin-1 (KHC) and B) Kinesin-2 (KIF3A/B) to assess motor processivity and ensure single molecule interactions. Data were fit to the Poisson distribution, where $P(n \geq 1) = 1 - \exp(-x/k)$. The fit gave k = 9.2 for Kinesin-1 and k = 5.9 for Kinesin-2.

Comparison of KIF3A/B Run Length to Previous Studies

The KIF3A/B run length measured here (449 ± 30 nm (mean ± SEM, n = 88)) was 3-fold less than that obtained by Berezuk et. al. using native chick embryo brain Kinesin-2 [6]. We believe that this difference results solely from the method of analysis, as follows. The present run length data were fit to a single exponential, while Berezuk et. al. computed their run length by taking the mean of all measured runs longer than 750 nm (their minimum detection limit). If a processive run is treated as a series of sequential and independent steps, then the mean run length can be computed by taking an arbitrary distance (i.e. the minimum detectable run length) and calculating the mean run length beyond

that distance. Subtracting 750 nm from the 1260 nm reported by Berezuk and Schroer gives a run length of 510 nm with a matching standard deviation of 560 nm, as expected for an exponential distribution [6]. The velocities of both KIF3A/B and KHC were in the same range as those reported by Berezuk and Schroer [6].

Interpreting KIF3A/B Run Length in Terms of Homodimer Run Lengths

Interestingly, the degree of processivity differed for the two homodimers – KIF3A/A (410 ± 35 nm, n = 85) was less processive than wild-type KIF3A/B (436 ± 129 nm/s, n = 90), while KIF3B/B (704 ± 81, n = 83) was more processive than wild-type. Because the homodimers were engineered by splicing at the neck-linker/neck-coil junction [1], the two homodimers possess identical coiled-coil stalks, suggesting that these functional differences arise solely due to differences in the head domains. Can the behavior of the heterodimer be quantitatively accounted for in terms of the behavior of the respective heads? If the two heads are assumed to behave identically and each step is history independent, then the probability of detachment per step is simply the inverse of the mean number of steps per run. Hence, during each step the probability of KIF3A/A detaching from the microtubule (p_A = 0.020) is almost twice that for KIF3B/B (p_B = 0.011). However, for a heterodimeric motor, where one head may have a higher detachment probability than the other head, predicting the run length from the detachment probabilities of each head is more complex.

To predict the run length of the KIF3A/B heterodimer from run lengths of the KIF3A/A and KIF3B/B homodimers, a probability model was developed as follows. Let ERL_A and ERL_B be the expected run lengths of the KIF3A/B motor when the motor first binds with the KIF3A head or the KIF3B head, respectively. If there is an equal probability of the motor initiating a run with either head, then the expected run length of KIF3A/B is a simple average of ERL_A and ERL_B.

$$ERL_{AB} = \frac{ERL_A + ERL_B}{2}$$

If a motor starts a run with head A and makes one step, then assuming history independence, the expected run length is ERL_B plus one step. Hence, the expected run length when the motor starts with head A is equal to the probability of detaching on the first step (p_A) times 1 step plus the probability of *not* detaching on the first step ($1-p_A$) times the expected run length if the motor completes that first step:

$$ERL_A = p_A \times 1 + (1 - p_A) \times (ERL_B + 1)$$

By symmetry, the equation for ERL_B can be expressed in terms of p_B and ERL_A, giving two equations with two unknowns, ERL_A and ERL_B. Solving these and taking their average gives the expected run length of KIF3A/B:

$$ERL_{AB} = \frac{4 - p_A - p_B}{2 \times (p_A + p_B - p_A p_B)}$$

Plugging in p_A = 0.020 and p_B = 0.011 from the homodimer experiments, the expected run length of KIF3A/B is calculated to be 64 steps, which is within two standard errors of the measured 56 +/- 4 steps for KIF3A/B (Table S1).

It has been established previously that in cells KIF3A can dimerize either with KIF3B or with KIF3C [7], and one possibility is that these different heterodimers possess different degrees of processivity. Because runs are limited by the least processive head, one implication is that KIF3A/C is at most only minimally more processive than KIF3A/B, although it could be significantly less processive.

Model Simulations

The stochastic models were developed in MATLAB, incorporating rate constants between different chemo-mechanical states. According to the Gillespie algorithm, for each state, the time to transition to the next state is given by:

$$t = \frac{1}{k} \ln \frac{1}{rand\#}$$

where k is the first order rate constant and rand# is a random number between 0 and 1 [8]. Beginning with motor binding in State 2, the transition time to each adjacent state was calculated, the state was updated, and the process repeated until the motor detached. An 8 nm step is associated with the transition from State 4 to State 1 (Figure 1) or State 7 to State 1 (Figure 4). 10,000 motor runs were simulated for each condition and the mean velocity and run length calculated. To identify the parameter set that most closely fit the experiments, experimental data across all ATP concentrations were plotted as run length versus velocity (as in Figure 5E) and fit by a line. The simulated run length and velocity values were compared to this line and the parameter set that gave the lowest R-squared was chosen. Parameters used in the final fits are given in Table S2.

Table S2: Rate Constants for Stochastic Simulations

Rate Constant	KHC (Fig. 1)	KIF3A/A (Fig. 4)	Notes
k_{detach}	250 s^{-1}	250 s^{-1}	Empirical
k'_{detach}	0.1 s^{-1}	0.1 s^{-1}	1/1000 of k_{detach}
k_{on}(ATP)	2 $\mu M^{-1}s^{-1}$	3 $\mu M^{-1}s^{-1}$	Refs [9, 10]
k'_{on}(ATP)	200 s^{-1}	15 s^{-1}	Adjusted to fit K_M(ATP)
$k_{hydrolysis}$	280 s^{-1}	120 s^{-1}	Refs [10, 11]
$k'_{hydrolysis}$	3.5 s^{-1}	3.5 s^{-1}	Ref [12]
k_{attach}	370 s^{-1}	370 s^{-1}	Adjusted to fit RL; ref [10]
k'_{attach}	0.1 s^{-1}	0.1 s^{-1}	1/1000 of k_{attach}
$k_{fhdetach}$	N.A.	11 s^{-1}	Refs [13, 14]
k_{unbind}	1.7 s^{-1}	2.3 s^{-1}	Refs [13, 15]
k_{unbind_2}	0.003 s^{-1}	0.003 s^{-1}	Refs [13-15]

Table S2: Final parameters used in the stochastic simulation of motor run length and velocity data. The model shown in Figure 1A was used for KHC and the model shown in Figure 4A was used for KIF3A/A. k′ denotes reverse rate constants; $k'_{fhdetach}$ was set to zero.

Comments on Rate Constants Used in Kinetic Simulations

Because the experimental data in this study are insufficient to constrain all of the kinetic parameters in the models presented Figures 1 and 4, selected model parameters were chosen from the literature. As there is considerable disagreement in the literature about the kinetic details of the Kinesin-1 hydrolysis cycle (for example, there is no agreement on the rate limiting step in the unloaded Kinesin-1 cycle), there are few "consensus" rate constants to choose from. The intent of our modeling

is to demonstrate that the structure of the Kinesin-1 model is incompatible with the Kinesin-2 data, necessitating a second detachment pathway, and we consider our chosen rate constants as a reasonable starting point that can be optimized by future modeling and experimentation.

A few of the chosen rate constants warrant further discussion. The overall KHC stepping rate of 88 s^{-1} (= 703 nm/s ÷ 8 nm/step) sets a lower limit of ~100 s^{-1} for any forward rate constant in the cycle. In the model structure in Figure 1, there are two predominant rate limiting steps – detachment of the trailing head (k_{detach} = 250 s^{-1}) and ATP hydrolysis ($k_{hydrolysis}$ = 280 s^{-1}), with some contribution from attachment of the tethered head (k_{attach} = 370 s^{-1}). From global fitting to the entire hydrolysis cycle, k_{detach} has been estimated to be ~50 s^{-1} by Gilbert et al. [16] or >100 s^{-1} by Hackney [10]. Using a cys-lite human construct, Rosenfeld et al. [17] measured the serial steps of ATP hydrolysis and rear head detachment at approximately 50 s^{-1}, although the 87 s^{-1} stepping rate of this same construct (700 nm/s) suggests that this value is an underestimate. Finally, FRET measurements by Mori et al. [18] that indicate kinesin is predominantly in a two-head bound state in 1 mM ATP, suggest that k_{detach}^{ADP} may the rate limiting step in the cycle. Hence, while our fit of 250 s^{-1} for k_{detach} is faster than most estimates, it is hard to argue that is the rate is any more than 2-fold slower than this. Our $k_{hydrolysis}$ of 280 s^{-1} is consistent with Gilbert et al. and Hackney [10, 11]. Finally, our k_{attach} of 370 s^{-1} is consistent with the 360 s^{-1} measured for ATP induced mantADP release from a docked motor by Hackney [10], although others have estimated this rate to be 2-fold or more slower [19, 20] or 2-fold faster [21].

In the Kinesin-1 hydrolysis cycle presented in Figure 1, the degree of processivity is determined by the relative rates of k_{attach} and k_{unbind} (probability of detachment = $k_{unbind}/(k_{unbind} + k_{attach})$). The ~2 s^{-1} detachment rate in the ADP state (giving a detachment probability of 0.005 per step) is somewhat slower than the 13 s^{-1} measured by Hackney [10] or the 42 s^{-1} estimated by Crevel et al. [22] from turbidity experiments. However, it is consistent with measurements by Hancock and Howard (3 s^{-1}) [15] and Uemura et al. (1 s^{-1}) [13], and it is consistent with recent results by Yildiz et al. who showed that in 1 mM ADP, a 2 pN rearward load causes a motor to walk backwards at 5 steps/s and a 1 pN forward load causes a motor to walk forward at 12 steps/s [14].

References

1. Zhang, Y., and Hancock, W.O. (2004). The two motor domains of KIF3A/B coordinate for processive motility and move at different speeds. Biophys J *87*, 1795-1804.
2. Williams, R.C., Jr., and Lee, J.C. (1982). Preparation of tubulin from brain. Methods Enzymol *85 Pt B*, 376-385.
3. Hyman, A., Drechsel, D., Kellogg, D., Salser, S., Sawin, K., Steffen, P., Wordeman, L., and Mitchison, T. (1991). Preparation of modified tubulins. Methods Enzymol *196*, 478-485.
4. Svoboda, K., Schmidt, C.F., Schnapp, B.J., and Block, S.M. (1993). Direct observation of kinesin stepping by optical trapping interferometry. Nature *365*, 721-727.
5. Block, S.M., Goldstein, L.S., and Schnapp, B.J. (1990). Bead movement by single kinesin molecules studied with optical tweezers. Nature *348*, 348-352.
6. Berezuk, M.A., and Schroer, T.A. (2007). Dynactin enhances the processivity of kinesin-2. Traffic *8*, 124-129.
7. Yang, Z., and Goldstein, L.S. (1998). Characterization of the KIF3C neural kinesin-like motor from mouse. Mol Biol Cell *9*, 249-261.
8. Gillespie, D.T. (1977). Exact stochastic simulation of coupled chemical reactions. J. Phys. Chem. *81*, 2340-2361.
9. Cross, R.A. (2004). The kinetic mechanism of kinesin. Trends Biochem Sci *29*, 301-309.

10. Hackney, D.D. (2002). Pathway of ADP-stimulated ADP release and dissociation of tethered kinesin from microtubules. implications for the extent of processivity. Biochemistry *41*, 4437-4446.
11. Gilbert, S.P., and Johnson, K.A. (1994). Pre-steady-state kinetics of the microtubule-kinesin ATPase. Biochemistry *33*, 1951-1960.
12. Hackney, D.D. (2005). The tethered motor domain of a kinesin-microtubule complex catalyzes reversible synthesis of bound ATP. Proc Natl Acad Sci U S A *102*, 18338-18343.
13. Uemura, S., Kawaguchi, K., Yajima, J., Edamatsu, M., Toyoshima, Y.Y., and Ishiwata, S. (2002). Kinesin-microtubule binding depends on both nucleotide state and loading direction. Proc Natl Acad Sci U S A *99*, 5977-5981.
14. Yildiz, A., Tomishige, M., Gennerich, A., and Vale, R.D. (2008). Intramolecular strain coordinates kinesin stepping behavior along microtubules. Cell *134*, 1030-1041.
15. Hancock, W.O., and Howard, J. (1999). Kinesin's processivity results from mechanical and chemical coordination between the ATP hydrolysis cycles of the two motor domains. Proc Natl Acad Sci U S A *96*, 13147-13152.
16. Gilbert, S.P., Moyer, M.L., and Johnson, K.A. (1998). Alternating site mechanism of the kinesin ATPase. Biochemistry *37*, 792-799.
17. Rosenfeld, S.S., Fordyce, P.M., Jefferson, G.M., King, P.H., and Block, S.M. (2003). Stepping and stretching. How kinesin uses internal strain to walk processively. J Biol Chem *278*, 18550-18556.
18. Mori, T., Vale, R.D., and Tomishige, M. (2007). How kinesin waits between steps. Nature *450*, 750-754.
19. Crevel, I., Carter, N., Schliwa, M., and Cross, R. (1999). Coupled chemical and mechanical reaction steps in a processive Neurospora kinesin. EMBO J *18*, 5863-5872.
20. Ma, Y.Z., and Taylor, E.W. (1997). Interacting head mechanism of microtubule-kinesin ATPase. J Biol Chem *272*, 724-730.
21. Rosenfeld, S.S., Xing, J., Jefferson, G.M., Cheung, H.C., and King, P.H. (2002). Measuring kinesin's first step. J Biol Chem *277*, 36731-36739.
22. Crevel, I.M., Nyitrai, M., Alonso, M.C., Weiss, S., Geeves, M.A., and Cross, R.A. (2004). What kinesin does at roadblocks: the coordination mechanism for molecular walking. Embo J *23*, 23-32.